Propulsion and Energy Forum
July 28-30, 2014, Cleveland, OH
50th AIAA/ASME/SAE/ASEE Joint Propulsion Conference

Propulsion System Design for a Martian Atmosphere Breathing Supersonic Retropropulsion Engine

Keir C. Gonyea[1] and Robert D. Braun[2]
Georgia Institute of Technology, Atlanta, GA, 30332

Design and analysis was performed on an atmospheric breathing propulsion system to land large-scale spacecraft on Mars. Initial feasibility of the engine was investigated analytically by employing equilibrium combustion and finite rate kinetics simulations in addition to 1st order propellant mass and inlet sizing. I_{SP} values (based on total propellant usage) were determined to be on the order of 120s-160s for onboard subsystems having a 10-to-1 oxidizer compression ratio. This corresponds to an I_{SP} of 600s-800s based on fuel consumption. While Mg-CO_2 mixtures have significant ignition constraints, favorable conditions were found, yielding ignition delay times of less than 1ms, by simultaneously employing designs exploiting both large reentry Mach numbers and modest compression ratios. These combinations allow for combustion to occur within moderately sized combustion chambers. The 1st order sizing calculations confirmed that atmospheric breathing supersonic retropropulsion has the potential for significant mass savings over traditional retropropulsion architectures. Engines sized with an oxidizer-to-fuel ratio of 4 require half the propellant consumption for an equivalent change in velocity. Inlet capture areas of the examined atmospheric breathing propulsion systems were on the order of the corresponding entry vehicle projected area. Therefore, this study envisioned an annular inlet design, which encircled the vehicle forebody. The aforementioned analyses address some of the challenges that need to be solved in order to ultimately obtain a practical atmospheric breathing supersonic retropropulsion system for Mars descent.

[1] Graduate Research Assistant, School of Aerospace Engineering, keir@gatech.edu
[2] David and Andrew Lewis Professor of Space Technology, School of Aerospace Engineering, robert.braun@aerospace.gatech.edu, AIAA Fellow

Nomenclature

α	Temperature preheat ratio
A	Integration matrix
c_p	Specific heat at constant pressure
D	Diameter
d	Initial solid droplet diameter
G	Gibbs free energy
g_e	Acceleration due to gravity on Earth
h	Enthalpy
I_{SP}	Specific Impulse
K	Equilibrium constant
M	3rd body specie
m	Mass
n	Number of moles
OF	Oxidizer-to-fuel ratio (by mass)
P	Pressure
P_i	Partial pressure (for gasses) or fugacity (for condensed species)
R	Universal gas constant
S	Entropy
T	Temperature
t	Burning time of a solid droplet
V	Volume
v	Velocity
X	Specie concentration

Subscripts

a,b,c	Stoichiometric coefficient of constituent atomic gas
comb	Property at the engine combustor
eff	Scaled by the oxidizer-to-fuel ratio
exit	Property at the nozzle exit
f	Property of the fuel
final	Property and the end of the simulation
i	Property of individual specie
induction	Property at the induction point
initial	Property at the beginning of the simulation
inlet	Property at the engine inlet
ox	Property of the oxidizer
p	Property of the entry vehicle propellant
ref	Property at reference conditions
s	Property of the entry vehicle structure
T	Property at a given temperature
tot	Total property over all species
veh	Property of the entry vehicle
X,Y,Z	Constituent atomic gas

Superscripts

0	Property at standard pressure
1	Property before fuel preheating
2	Property after fuel preheating
*	Property of the entry vehicle payload

Acronyms

AB-SRP	Atmospheric Breathing Supersonic Retropropulsion
MT	Metric ton (1000 kg)
SRP	Supersonic Retropropulsion

I. Introduction

The exploration of Mars has progressed significantly over the last half century. Much of this is due to the missions carried out by landers and rovers such as Viking, Pathfinder, Mars Exploration Rovers and Phoenix. Each of these missions was successful in safely entering the Mars atmosphere and landing on the planet's surface. However, the Mars Science Laboratory has pushed the extent of landing capabilities on Mars using incremental advances of Viking-technology, placing limitations on the mass, landing location and landing accuracy of an entry vehicle.[1] Attempting to land heavier payloads would, among other factors, require an increase in the size of the supersonic parachute decelerator system beyond its presently qualified limits. Therefore, in order to continue to progress and send heavier payloads to Mars it is necessary to develop new technologies to increase current atmospheric descent and landing capabilities. This is also required in order to enable future human-precursor and human-scale missions (10+ MT) to Mars.[1]

One possible technology to enable future high mass missions to Mars is the use of Supersonic Retropropulsion (SRP). SRP involves using thrusters directed in opposition to the oncoming airflow to decelerate the entry vehicle while it is traveling at supersonic speeds. SRP has been shown to be attractive as a Mars descent solution because, while it is affected by the scaling requirements that come with increasing payload masses, it is a technology solution that conceptually scales across a wide range of vehicle systems. However, SRP systems increase the entry mass (and potentially the volume) of spacecraft because it is necessary to store the fuel and oxidizer onboard the vehicle. For example, a SRP vehicle to land humans on Mars (40 MT payload) is expected to require 12 MT of propellant, 2.5 MT of fuel and 9.5 MT of oxidizer.[2] Because of this propellant mass required, currently proposed SRP configurations require a significant increase in performance before they will be seriously considered for Mars missions.

One possible solution to the problem of SRP mass is the use of an atmospheric-breathing propulsion system for the SRP thrusters. An atmospheric-breathing propulsion system, unlike a conventional rocket propulsion system, does not carry the oxidizer within the craft itself. It instead ingests the oxidizer from the surrounding atmosphere and combines it with the fuel carried onboard to create thrust. Because the oxidizer is not carried within the vehicle this significantly reduces the mass requirements of the entry system. This efficiency is illustrated in the significantly higher *Isp* of atmospheric-breathing propulsion systems relative to rocket propulsion systems over the range of applicable Mach numbers.[3] In the case of a Mars lander, this oxidizer would have to be carried throughout the entirety of the mission (from launch or Earth departure until Mars descent); as such, its elimination from the vehicle would result in a significant performance advantage.

One challenge with using an atmospheric-breathing supersonic retropropulsion (AB-SRP) system on Mars is that the Martian atmosphere consists largely of carbon dioxide (CO_2), not air. Thus, traditional oxygen combustion is not possible. Instead, innovative combustion techniques need to be assessed and developed that allow for combustion using CO_2 as an oxidizer. Magnesium (Mg) is the most popular fuel for burning in CO_2 due to its high I_{SP} at high oxidizer-to-fuel ratios.[4,5] This allows Mg-CO_2 engines to reduce onboard propellant mass. In addition, Mg combusts readily in CO_2 flows and has low proportions of condensed phase products, both of which are favorable for a reliable engine.[6] The initial feasibility of such propulsion systems have been demonstrated by the Wickman Spacecraft & Propulsion Company and Pioneer Aerospace, each having shown the production of thrust in a rocket engine that combusts magnesium powder with CO_2.[7,8] The potential performance of AB-SRP engines is investigated further in this paper.

II. Methodology and Results

A. Equilibrium Combustion Simulation

1. Methodology

An equilibrium combustion simulation was written to calculate the ideal I_{SP} of a Mg-CO_2 engine. The I_{SP} values are an important metric to compare different engines and combustion parameters as well as to calculate the vehicle thrust in future trajectory simulations. These data were used for rapid first order sizing estimates of the propulsion system and entry vehicle.

The I_{SP} of an engine is defined by Eq. (1), where v_{exit} is the gas exit velocity and g_e is the acceleration due to gravity on Earth. The exit velocity can be calculated via Eq. (2) with h being the enthalpy of the mixture, calculated from the equilibrium combustion simulation. Since the AB-SRP engine is an atmospheric breathing engine, the I_{SP} value can be rescaled by the fuel-oxidizer ratio (*OF)* as in Eq. (3) to determine the effective I_{SP}, which accounts for the fact that the AB-SRP vehicle does not carry its own oxidizer. $I_{SP,eff}$ values are a better metric to use when

comparing against traditional rocket engines since they are solely based on the propellant carried onboard the vehicle.

$$I_{SP} = \frac{v_{exit}}{g_e} \tag{1}$$

$$v_{exit} = \sqrt{2\left(h_{inlet} - h_{exit}\right)} \tag{2}$$

$$I_{SP,eff} = I_{SP}\left(1 + OF\right) \tag{3}$$

The equilibrium combustion simulation is a variant of the method developed by Huff, Gordon, and Morrell and is able to calculate the equilibrium composition and temperature of gas and condensed phase mixtures.[9] The method iteratively converges on the solution by enforcing the conservation equations. The gas phase species are assumed to be ideal gasses, defined by Eq. (4), and the condensed phase species are assumed to have partial pressures of 0 and fugacity of 1. In these equations P is pressure, n is number of moles, V is volume, R is the gas constant, and T is temperature.

$$P_{i,gas} = n_i \frac{V}{RT} \tag{4}$$

The modeling of a given reaction product created from its associated constituent gasses is governed by Eq. (5) and the equilibrium condition for the partial pressures of the species is given by Eq. (6). For condensed phase species the P_i in Eq. (6) refers to its associated fugacity, which is 1. The equilibrium constant is obtained using Eq. (7). In these equations a and b are both the number of moles of constituent gasses Z and Y, respectively, as well as the number of Z and Y atoms in the product molecule. Note that K denotes the equilibrium constant and ΔG_T^0 is the difference in the Gibbs free energy between the product molecule and constituent gasses at the given temperature and standard pressure.

$$a_i Z + b_i Y + \ldots \rightarrow Z_{a_i} Y_{b_i} \ldots \tag{5}$$

$$K_i = \frac{P_i}{P_Z^{a_i} P_Y^{b_i} \ldots} \tag{6}$$

$$K_i = e^{\left(\frac{-\Delta G_T^0}{RT}\right)_i} \tag{7}$$

The remaining constraints on the solution conserve mass, defined by Eq. (8), constrain the static pressure, defined by Eq. (9), and satisfy energy conservation, defined by Eq. (10). Eq. (10) is replaced by a constant entropy condition for calculations modeling an isentropic expansion process, seen in Eq. (11). In these equations T_{ref} is a reference temperature, c_P is the specific heat at constant pressure, $h_{T_{ref}}$ is the enthalpy of formation, and S_T^0 is the entropy at standard pressure. For condensed phase species the P_i in Eq. (11) refers to their fugacity.

$$a_{prod} = \sum_{reac} a_i n_i \tag{8}$$

$$P = \sum P_i \tag{9}$$

$$\sum_{reac} n_i \left(\int_{T_{ref}}^{T} c_P \, dT + h_{T_{ref}} \right) = \sum_{prod} n_i \left(\int_{T_{ref}}^{T} c_P \, dT + h_{T_{ref}} \right) \tag{10}$$

$$\sum_{reac} n_i \left(S_T^0 - RP_i \ln\left(P_i\right) \right) = \sum_{prod} n_i \left(S_T^0 - RP_i \ln\left(P_i\right) \right) \tag{11}$$

Data for the thermodynamic properties of each specie were obtained from the NASA Report 3001.[10]

2. Validation

Previous studies have calculated the I_{SP} values of a Mg-CO_2 engine to be used on Mars for a range of oxidizer-to-fuel ratios.[4,5,11] The literature calculations were originally only used to assess different fuels for a metal-CO_2 engine and to select a specific fuel for future study. However, since the absence of a parameterized study made it hard to use their data in higher fidelity simulations, it was necessary to develop an independent simulation to determine the engine I_{SP} over a range of composition, pressure and temperature. Hence, these simulations served as validation test cases.

The previous studies assumed combustion chamber and expansion pressures of 10 bar and 10 mbar, respectively, consistent with values for a Mars "hopper" or other surface vehicle. However, the reports did not mention the initial gas temperature for the calculations, which affects the I_{SP} results. An equilibrium simulation was developed to calculate the I_{SP} values for the specified pressures and a range of initial gas temperatures to evaluate which temperature best correlated with the literature values. The results of the simulation, seen in Fig. 1, show the calculated I_{SP} values for an initial temperature of 200K. Of all the temperature values tested, 200K best compares with the data reported in the literature. Note that the data generated in this study also compare well with those of other Mg-CO_2 engine studies available in the literature.

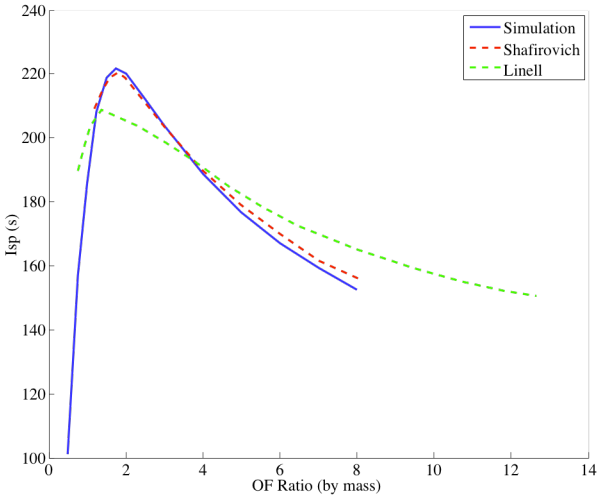

Figure 1. Validation of I_{SP} calculations with literature results

3. Results

The atmospheric conditions for the literature studies, which focused primarily on surface vehicles, are significantly different to the conditions for an entry vehicle. Therefore, the equilibrium simulation was run for a range of pressures and temperatures to calculate the I_{SP} values in a relevant flight regime and to investigate where the AB-SRP engine would be effective. These results will serve as a comparison to traditional rocket engines and will be used in conjunction with a future trajectory simulation to design a propulsion system that minimize the entry vehicle mass while still landing safely.

Two points were chosen on the Mars Science Laboratory trajectory (payload mass of 1 MT) at M = 1 and M = 4.[12] It was assumed that the freestream air at these points passed through a normal shock before being isentropically compressed by some onboard process.[13,14,15] Combustion occurred at the post-compression pressure and the mixture was expanded to the post-shock pressure. Two parameters were varied during the simulation, the isentropic compression pressure ratio and the fuel temperature preheating ratio. The pressure ratio, defined as P_{comb}/P_{inlet}, denotes the amount of inlet compression and was varied from 1 to 100. The temperature ratio, defined as $\alpha = (T_f^2 - T_f^1)/(T_{ox} - T_f^1)$, scales the temperature of the preheated fuel (T_f^2) between its storage temperature (T_f^1) when $\alpha = 0$ and the compressed oxidizer temperature (T_{ox}) when $\alpha = 1$. The composition was fixed at OF = 4 since previous literature studies indicated this would balance the large heat release of a near-stoichiometric mixture with the reduced fuel consumption of a large oxidizer-to-fuel ratio mixture.[4] Oxidizer freestream and post-shock states for the two trajectory points are shown in Table 1 and I_{SP} results are shown in Fig. 2.

Table 1. Oxidizer state prior to isentropic compression for both trajectory points

	Trajectory Point 1 (M = 1)		Trajectory Point 2 (M = 4)	
	Freestream	Post Shock	Freestream	Post Shock
Altitude (km)	5.4		12.8	
Pressure (kPa)	0.43	0.43	0.22	3.96
Temperature (K)	236.7	236.7	221.3	751
Density (kg/m^3)	0.0094	0.0094	0.0051	0.0271
Velocity (m/s)	257	257	800	174

As seen in Fig. 2, the I_{SP} values are primarily sensitive to the temperature ratio for large compression ratios. As a result, complex systems to preheat the fuel are not necessary to improve the engine thrust. However, since the magnesium will be stored onboard as a solid another reason for preheating the fuel would be to vaporize the particles. This would improve the combustion kinetics and drastically decrease the induction time before burning. The boiling point of magnesium is 1363K. For perfect fuel preheating, this requires pressure ratios of 1633 and 12.5 for the $M = 1$ and $M = 4$ trajectory points, respectively. Other sources of heat may be available since the adiabatic flame temperature of representative Mg-CO_2 flames is approximately 3000K and the surface temperatures of entry vehicles will be in the 1000's of Kelvin. The need and engineering feasibility of exploiting these sources will be analyzed in future studies.

The I_{SP} values are sensitive to the compression ratio. This is to be expected since the difference in pressure between the combustion chamber and exit drives the increase in gas velocity. As displayed in both Figs. 2a and 2b, a pressure ratio of 5 is required before there is any appreciable I_{SP} generated whereas, a pressure ratio of 10 is required to achieve I_{SP} values that are significant. For the $M = 1$ trajectory point, the total pressure (maximum possible pressure from inlet compression) corresponds to a 1.8 compression ratio. For the $M = 4$ trajectory point, the freestream total pressure corresponds to a 10.8 pressure ratio and the post-shock total pressure corresponds to a 1.1 pressure ratio. This indicates that additional onboard compression will be required since inlet compression alone is not expected to provide a sufficient pressure rise. However, compression ratios above 10-to-1 result in a diminishing return on I_{SP}, with only 40% increase in I_{SP} for 900% increase in pressure ratio. The amount of compression necessary (and obtainable) will also be investigated in future studies.

The advantage of an airbreathing engine is seen in Figs. 2c and 2d. For an engine with an *OF* ratio of 4 the $I_{SP,eff}$ (based on fuel consumption) is 5 times greater than the I_{SP} value (based on total propellant usage). Therefore, while the I_{SP} of an AB-SRP engine may only be 120s, one third that of a typical SRP engine (I_{SP} of 370s for a liquid oxygen, liquid methane engine), its I_{SP} based off of propellant consumption is 600s, over one and a half times that of the SRP engine.[16] These results demonstrate that AB-SRP has the potential to be a feasible component for large mass Mars missions.

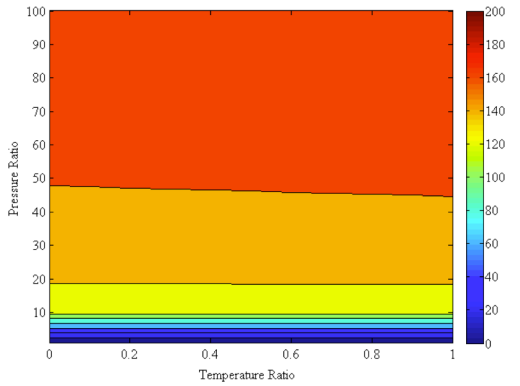

(a) I_{SP} values for the $M = 1$ trajectory point (s)

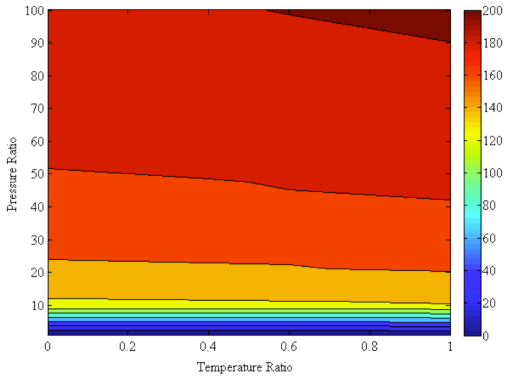

(b) I_{SP} values for the $M = 4$ trajectory point (s)

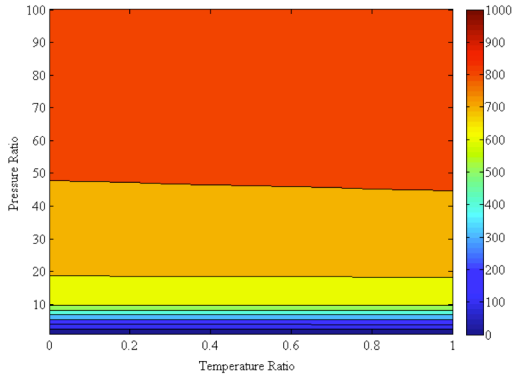

(c) $I_{SP,eff}$ values for the $M = 1$ trajectory point (s)

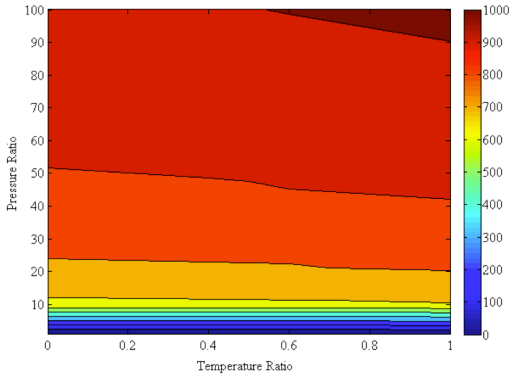

(d) $I_{SP,eff}$ values for the $M = 4$ trajectory point (s)

Figure 2. I_{SP} values (in seconds) for the $M = 1$ and 4 trajectory points as a function of isentropic compression pressure ratio and fuel temperature preheating ratio

B. Finite Rate Kinetics Simulation

1. Methodology

A finite rate kinetics simulation was written to calculate the time dependent temperature and composition of the combustion process. This was necessary to size the length of the propulsion system and determine the effects of pressure and temperature on combustion. For the simulation, it was assumed that the fuel and oxidizer would enter the combustor perfectly mixed and at the same temperature based on the total enthalpy of the reactants. The intermediate reactions and their corresponding rate constants were obtained from the literature and are shown in Eq. (12).[17] In these equations, *M* denotes a 3rd body specie. Thermodynamic tables do not typically differentiate between condensed phases of magnesium oxide (MgO).[10] Therefore, this study ignored Eq. (12f) and interpreted MgO(l) as a condensed phase in Eq. (12e). Note that the inclusion of carbon (C) in Eqs. (12b) and (12j) made the integration scheme unstable. Therefore, Eq. (12j) was ignored and carbon was introduced into the system in partial equilibrium according to Eq. (12b), which was the faster of the two reactions.

$$Mg + CO_2 \leftrightarrow MgO + CO \tag{12a}$$
$$Mg + CO \leftrightarrow MgO + C \tag{12b}$$
$$Mg + O_2 \leftrightarrow MgO + O \tag{12c}$$
$$Mg + O + M \leftrightarrow MgO + M \tag{12d}$$
$$MgO \leftrightarrow MgO(l) \tag{12e}$$
$$MgO(l) \leftrightarrow MgO(s) \tag{12f}$$
$$Mg + CO_2 \leftrightarrow MgO + CO \tag{12g}$$
$$2O + M \leftrightarrow O_2 + M \tag{12h}$$
$$CO + O + M \leftrightarrow CO_2 + M \tag{12i}$$
$$C + O_2 \leftrightarrow CO + O \tag{12j}$$

From the elementary reaction equations it was possible to set up a 1st order system of ordinary differential equations of the form of Eq. (13). In this equation, $\vec{X}$ is the vector of all of species concentrations and A is a square matrix. A is specific to a given set of elementary equations and is a function of the forward and backward rate constants of those equations and the current specie concentrations. A Runge-Kutta 4 method was used to integrate Eq. (13) forward in time.

$$\frac{d\vec{X}}{dt} = A\vec{X} \tag{13}$$

The temperature and volume of the mixture were calculated by enforcing conservation of mass and energy at each iteration using Eqs. (14) and (15). In these equations a_{tot} is the total number of moles of a given atom and h_{tot} is the total enthalpy of the system. V is the total volume of gas.

$$a_{tot} = V\sum X_i a_i \tag{14}$$
$$h_{tot} = V\sum X_i h_{T,i} \tag{15}$$

The finite rate kinetics simulation was validated by checking the conservation of mass and energy at each iteration and by comparing the steady state solution to that obtained from the equilibrium combustion simulation.

2. Ignition Results

A study was performed to calculate the ignition delay of Mg-CO_2 mixtures for an AB-SRP vehicle. Four points were chosen on the MSL trajectory at M = 1, 2, 3, and 4. As in the equilibrium combustion simulation, the freestream carbon dioxide at these points passed through a normal shock and was isentropically compressed with pressure ratios varying between 1 and 100. The magnesium fuel was preheated up to the oxidizer temperature with ratios varying between 0 and 1. Both reactants were assumed to enter the combustion chamber at a single

temperature based on the mixture total enthalpy but the time required to equilibrate temperatures was considered to be instantaneous. This simulation only analyzed the case of $OF = 4$.

The simulation was run for a total of 0.1s. If the mixture had not reached steady state in that time it was recorded as having not combusted. The ignition point was chosen to be where the temperature had undergone ninety percent of its total increase, defined by Eq. (16). In Eq. (16), $T_{induction}$ is the temperature at ignition, $T_{initial}$ is the temperature at the beginning of the simulation and T_{final} is the maximum temperature.

$$T_{induction} = 0.9T_{final} + 0.1T_{initial} \tag{16}$$

Since an actual propulsion system would combust gaseous carbon dioxide with solid magnesium particles, these two species were chosen as the reactants. However, since no kinetics data was available on the burning or vaporization of Mg(s) the simulation started with both gaseous carbon dioxide and gaseous magnesium at a temperature equating the total enthalpy of the mixture to that of the reactants. The time required to convert the Mg(s) to Mg(g) was accounted for by adding an additional time for solid particle vaporization, seen in Eq. (17). This time is consistent with literature experiments or computation of Mg droplets burning in a CO_2 stream.[17,18,4,19] The burning times of a representative 100μm particle are shown next to their corresponding expressions, with a median time of 6.5ms. The units of Eq. (17) are in s and mm. t_b denotes the burning time and d is the initial droplet diameter.

Modak[17]	(in reduced gravity)	$t_b = 1.0d^2$	$t_b = 1\times10^{-2}\,s$	(17a)
	(in terrestrial gravity)	$t_b = 0.5d^2$	$t_b = 5\times10^{-3}\,s$	(17b)
Legrand[18]		$t_b = 0.5d^2$	$t_b = 5\times10^{-3}\,s$	(17c)
Shafirovich[4]		$t_b = 0.25d^{2.7}$	$t_b = 5\times10^{-4}\,s$	(17d)
King[19]	(with surface reactions)	$t_b = 0.83d^2$	$t_b = 8\times10^{-3}\,s$	(17e)
	(without surface reactions)	$t_b = 3.1d^2$	$t_b = 3\times10^{-2}\,s$	(17f)

Out of all of the trajectory points, compression ratios, and preheat amounts no Mg(s)-CO_2 mixture combusted within 0.1s. Therefore, it will be necessary to either vaporize the magnesium particles prior to combustion or include an igniter to start the engine.

A second study was performed that combusted gaseous magnesium and carbon dioxide reactants. Reactant pressures and temperatures were the same as for the Mg(s)-CO_2 simulations. None of the mixtures combusted within 0.1s for the $M = 1$ and 2 trajectory points. However, since the AB-SRP initiation will likely occur at higher Mach numbers this is not a relevant problem. Induction delays for the $M = 3$ and 4 trajectory points are shown in Fig. 3 with the log base 10 value of induction delay (in seconds) plotted against the compression pressure ratio and preheat temperature ratio. The values of both graphs are clipped at 0.1s to indicate that combustion did not occur.

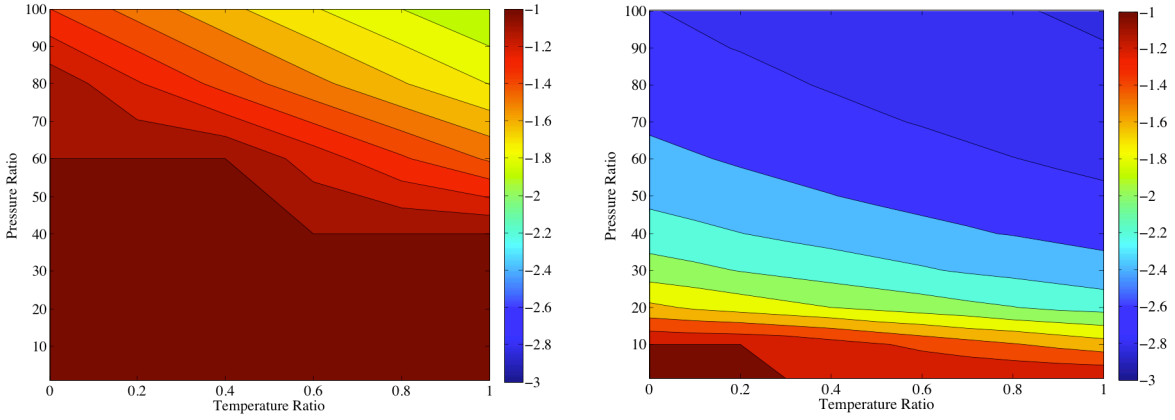

(a) Induction time for the $M = 3$ trajectory point

(b) Induction time for the $M = 4$ trajectory point

Figure 3. Induction delay times for a Mg(g)-CO_2 mixture as a function of isentropic compression pressure ratio and fuel temperature preheating ratio. Colors represent log base 10 values of induction times in seconds.

As seen in Fig. 3, of the two parameters the induction times are more sensitive to the compression pressure ratio than the preheat temperature ratio. This is a similar result to what was seen in the equilibrium combustion simulations. From Fig. 3a, a significant amount of compression is needed in order to ignite the mixture at $M = 3$. Depending on the flowpath and residence time of the combustion chamber an igniter may still be required. As seen in Fig. 3b, reasonably fast induction delays are achieved at lower compression ratios. If higher compression ratios are attainable then the propulsion system could be self-starting. In addition, if the AB-SRP system is able to start at higher Mach numbers then the ignition times become even more favorable.

3. Burning Rate Results

After analyzing the propulsion system ignition characteristics, a final study was performed to investigate the burning rate of an existing Mg-CO_2 flame. For this study solid magnesium and gaseous carbon dioxide entered the combustion chamber at the adiabatic flame temperature, here assumed to be 3000K since representative Mg-CO_2 flames have an adiabatic flame temperature at or above 3000K. Before the simulation started the solid magnesium was assumed to have vaporized in a time consistent with Eq. (17). The simulation was run for pressures ranging between $4x10^{-3}$atm and 4atm, encompassing all of the pressures expected during the trajectory for all considered compression ratios and preheat ratios. For the current study the mixture ratio was set at $OF = 4$. Burning times for the different pressures are presented in Fig. 4. The burning times were calculated via Eq. (16) and do not include the assumed droplet vaporization time.

As seen in Fig. 4, burning times for all combustion pressures are below 1ms. This is promising and demonstrates that a Mg-CO_2 flame can burn within a reasonably sized combustion chamber. Actual sizing, however, will depend on the mixture velocity through the chamber and will be performed in later analyses. The burning times were expected to decrease with increasing pressure. However, Fig. 4 shows that burning times increase for pressures between 0.2 and 0.6 atm. By analyzing the temperature profiles versus time for each case it was discovered that the temperature asymptotically approached its steady state value for pressures above 0.6 atm. For pressures below 0.2 atm the temperature rapidly overshot steady state and slowly relaxed to the final temperature. For these cases, since the peak temperature corresponded to the maximum heat release and since the relaxation to steady state was sufficiently slow the maximum temperature was chosen as the burning point. Simulations conducted at pressures between 0.2 and 0.6 atm transitioned between the two temperature profiles. As was seen in the ignition simulation, variations in pressure caused larger fluctuations in induction delay than variations in temperature. Therefore, the results of Fig. 4 are not expected to change significantly with more accurate predictions of the adiabatic flame temperature.

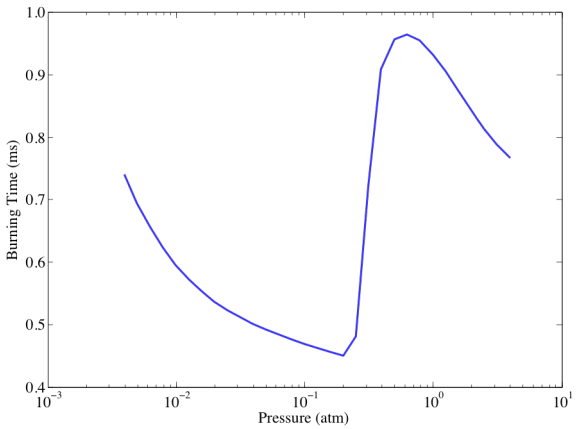

Figure 4. Mg-CO_2 flame burning times for various pressures expected during the trajectory

C. 1st Order Sizing

1. Methodology

A 1st order sizing calculation was performed that estimated the propellant mass and inlet area of an AB-SRP vehicle. Since the calculations do not consider losses or inefficiencies of the engine and inlets they are presented as rough vehicle sizing estimates to compliment the propulsion system results. Previous studies of human scale Mars entry vehicles (50MT dry mass) indicated that SRP initiation would occur at $M = 2.3$ at an altitude of 1350m, corresponding to an approximate velocity of 473m/s.[20] Therefore, the study sized an SRP and AB-SRP propulsion system to take a 50MT vehicle from 473 to 0m/s. The I_{SP} of the SRP vehicle, 370s, was based off a typical liquid oxygen, liquid methane engine.[2,16] The performance of the AB-SRP engine was based off the equilibrium combustion simulation results and estimated an I_{SP} of 120s or 160s at $OF = 4$ and I_{SP} of 160s at $OF = 2$. An I_{SP} of 120s seemed reasonable for the $M = 1$ trajectory point and $I_{SP} = 160$s seemed attainable for $M = 4$ or higher trajectory points. Since $OF = 2$ is closer to stoichiometric than $OF = 4$ an $I_{SP} = 160$s was assumed for the overall AB-SRP engine performance at $OF = 2$. Sizing of the SRP engine was performed using the ideal rocket equation in Eq. (18a). The propellant mass can be calculated via Eq. (18b). For the AB-SRP vehicle, the I_{SP} needs to be replaced

with the effective I_{SP}, resulting in Eqs. (18c) and (d). In Eq. (18) m_s refers to the structure mass, m^* refers to the payload mass, and m_p refers to the propellant mass.

$$\Delta v = -g_e I_{SP} \ln\left(\frac{m_s + m^*}{m_s + m^* + m_p}\right) \tag{18a}$$

$$m_p = e^{\frac{\Delta v}{g_e I_{SP}}}\left(m_s + m^*\right)\left(1 - e^{\frac{-\Delta v}{g_e I_{SP}}}\right) \tag{18b}$$

$$\Delta v = -g_e I_{SP}\left(OF + 1\right)\ln\left(\frac{m_s + m^*}{m_s + m^* + m_p}\right) \tag{18c}$$

$$m_p = e^{\frac{\Delta v}{g_e I_{SP}(OF+1)}}\left(m_s + m^*\right)\left(1 - e^{\frac{-\Delta v}{g_e I_{SP}(OF+1)}}\right) \tag{18d}$$

For the AB-SRP propulsion system, the oxidizer mass capture required can be calculated via Eq. (19). The inlet area and diameter can then be calculated via. Eqs. (20) and (21), respectively. Two inlet configurations are currently being considered. The first is a circular inlet at the entry vehicle nose, denoted as *'inner,'* and the second is an annulus surrounding the vehicle (entry vehicle diameter, D = 10m), denoted as *'outer*.'[20] The total mass of CO_2 in a column extending up from a point on the surface is 150kg/m^2.[21] Since an actual entry vehicle would be traveling laterally along the surface of Mars for a portion of its flight, this value was used as an order of magnitude estimate to size the inlets until higher fidelity simulations can provide a more accurate result.

$$m_{ox} = OF \cdot m_f \tag{19}$$

$$A_{inlet} = \frac{m_{ox}}{150\,{}^{kg}\!/_{m^2}} \tag{20}$$

$$D_{inlet,\,outer} = 2\left(\frac{A_{inlet} + \pi\left(\frac{D_{veh}}{2}\right)^2}{\pi}\right)^{1/2} \tag{21}$$

2. Results

Results of the study are shown in Table 2. Included in the table is a scale diagram of the annular inlet (*'outer'* design) area compared to the entry vehicle for each propulsion system configuration. It is important to note that this analysis did not take into account the difference in propulsion system mass of an AB-SRP system, any inefficiencies

Table 2. Required propellant mass and inlet area for various AB-SRP and SRP propulsion system configurations

	AB-SRP, OF = 4		AB-SRP, OF = 2	SRP
	I_{SP} = 120s	I_{SP} = 160s	I_{SP} = 160s	I_{SP} = 370s
m_p (MT)	4.19	3.11	5.29	6.79
A_{inlet} (m^2)	112	83	71	
D_{inlet} (inner) (m)	11.9	10.3	9.5	
D_{inlet} (outer) (m)	15.6	14.3	13.8	
Diagram Entry Vehicle Inlet	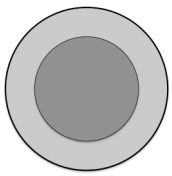	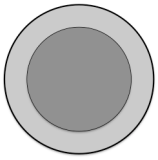	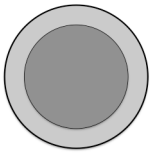	

of ingesting the oxidizer or the thrust variation throughout the trajectory. Nevertheless, the advantages of an atmospheric-breathing engine are clearly evident in the lower propellant mass requirements of all AB-SRP configurations. Since this analysis is idealized all of the propellant values are expected to be lower bounds. This may not be the case if the deceleration due to drag is on the order of that due to thrust for the AB-SRP vehicle, which will be investigated in future studies. For reference, the propellant mass for the SRP system is 12MT when calculated via higher fidelity analysis.[2]

The higher I_{SP} engine has a significant advantage in mass and inlet area, which is to be expected. However, since the I_{SP} will vary during the trajectory, the inlet would ultimately be sized between the two results. It can be seen that by varying the oxidizer-to-fuel ratio the propulsion system can trade propellant mass with inlet area. This parameter can therefore be tuned to balance the difficulty of carrying additional mass or including a larger inlet. Of all cases considered, the $OF = 2$ engine is the only configuration that allows for an inlet located at the nose of the entry vehicle since both $OF = 4$ cases result in the inlet diameter being larger than that of the vehicle itself. However, even this case is not practical since the inlet would cover 90% of the frontal area. The feasibility of designing an annular inlet of the required size will be analyzed in the future.

III. Conclusion

The overall feasibility and performance of an AB-SRP propulsion system is investigated through numerical simulation. Representative engines were seen to have sufficient I_{SP} values and burning rates and overall sizing of the AB-SRP system showed it to have the expected mass benefits over traditional SRP configurations with reasonably sized inlets.

An equilibrium combustion simulation was written to calculate the ideal I_{SP} of an AB-SRP propulsion system. Realistic I_{SP} values were around 120s-160s (corresponding to effective I_{SP} values of 600-800s), double that of a traditional SRP propulsion system when calculated based on onboard propellant consumption. Attaining these I_{SP} values will require a 10-to-1 compression of the oxidizer prior to combustion. This must be achieved using an onboard subsystem since the oxidizer total pressure is too small for effective inlet compression. Pressure ratios above 10-to-1 do not currently seem necessary since they provide diminishing benefit. In addition, preheating of the fuel does not provide any noticeable gain in the theoretical I_{SP} for reasonable compression ratios; however, it does significantly improve the combustion kinetics.

The finite rate kinetics simulation investigated the propulsion systems ability to ignite and maintain a flame. The Mg(s)-CO_2 mixture did not ignite for any of the trajectory points, pressure or temperature ratios. Therefore, either the magnesium needs to be vaporized prior to ignition or an igniter needs to be added to the engine. The Mg(g)-CO_2 mixture ignited for high Mach number initiation but required moderate compression. Simulation of the magnesium, carbon dioxide flame demonstrated that burning times were less than 1ms for all pressures expected throughout the trajectory. Therefore, maintaining a Mg-CO_2 flame appears feasible.

When sizing the AB-SRP and SRP propulsion systems to land a human-scale vehicle all of the AB-SRP configurations were more mass efficient than SRP, in which higher I_{SP} and higher oxidizer-to-fuel ratio engines presented the most benefit. However, high OF ratio engines also required larger inlets to ingest the atmosphere. None of the engines could support an inlet located at the stagnation point of the vehicle since all inlet diameters were on the order of the vehicle diameter. Therefore, entry architectures need to include inlets exterior to the vehicle or develop innovative ways of increasing the oxidizer mass capture.

Further work will be done to understand the performance of an AB-SRP propulsion system. Research into possible compression subsystems will determine what compression ratios are possible for the engine and what is the associated mass, size and power requirements. This will help determine the I_{SP} capabilities of the engine. Design of the inlet geometry and propellant flowpath will inform the velocity profile of the engine, which will determine the combustion chamber size. In addition, a better mass estimate of the AB-SRP system will be developed through trajectory and vehicle design work. This will also allow for a better determination of the inlet area and combustion parameters to minimize the mass of the entire system.

Acknowledgments

This research is funded by the NASA Science and Technology Research Fellowship (NSTRF). Many thanks to Dr. Aaron Auslender for his guidance and insight on the high level goals of the project and his invaluable help on the simulation development.

References

[1] R. D. Braun, and R. M. Manning. "Mars Exploration Entry, Decent and Landing Challenges." Journal of Spacecraft and Rockets 44.2 (2007): 310-23.

[2] K. T. Edquist, A. A. Dyakonov, A. M. Korzun, J. D. Shidner, J. W. Studak, M. A. Tigges, D. M. Kipp, R. Prakash, K. A. Trumble, and I. C. Dupzyk. "Development of Supersonic Retro-Propulsion for Future Mars Entry, Descent, and Landing Systems," AIAA Paper 2010-5046, June 2010

[3] W. Whitlow, R. A. Blech, and I. M. Blankson. "Innovative Airbreathing Propulsion Concepts for Access to Space." Novel Aero Propulsion Systems International Symposium (2000).

[4] E. Y. Shafirovich, A. A. Shiryaev, U. I. Goldshleger. "Magnesium and Carbon Dioxide: A Rocket Propellant for Mars Missions." Journal of Propulsion and Power Vol. 9, No. 2, March-April 1993.

[5] E. Shafirovich, and A. Varma. "Metal-CO2 Propulsion for Mars Missions: Current Status and Opportunities." 43rd Joint Propulsion Conference & Exhibit. 8 - 11 July 2007, Cincinnati, OH. AIAA 2007-5126.

[6] S. Yuasa, and H. Isoda. "Carbon Dioxide Breathing Propulsion for a Mars Airplane." 25th Joint Propulsion Conference. 10-12 July 1989. Monterey, CA. AIAA 89-2863.

[7] J. H. Wickman. "In-Situ Mars Rocket and Jet Engines Burning Carbon Dioxide." AIAA Paper 99-2409, June 1999**.**

[8] R. Zubrin, T. Muscatello, B. Birnbaum, K. M. Caviezel, G. Snyder, and M. Bergren. "Progress in Mars ISRU Technology," AIAA Paper 2002-0461, Jan. 2002.

[9] V. N. Huff, S. Gordon, and V. E. Morrell. "General Method and Thermodynamic Tables for Computation of Equilibrium Composition and Temperature of Chemical Reactions." NACA Report 1037.

[10] B. J. McBride, S. Heimel, J. G. Ehlers, and S. Gordon. "Thermodynamic Properties to 6000K for 210 Substances Involving the First 18 Elements." NASA SP-3001. 1963.

[11] J. A. Linnell, and T. F. Miller. " Preliminary Design of a Magnesium Fueled Martian Ramjet Engine," AIAA Paper 2002-3788, July 2002.

[12] C. D. Karlgaard, P. Kutty, J. Shidner, M. Schoenenberger, and M. M. Munk, "Mars Entry Atmospheric Data System Trajectory Reconstruction Algorithms and Flight Results," AIAA 2013-0028, 2013.

[13] T. Benson. "Mars Atmosphere Model". NASA Glenn Research Center. June 12, 2014.

[14] J. D. Anderson, "Fundamentals of Aerodynamics (4th ed.)." McGraw-Hill, 2007. ISBN 0-07-125408-0.

[15] G. J. Van Wylen, and R. E. Sonntag. "Fundamentals of Classical Thermodynamics." John Wiley & Sons, Inc., New York, 2007. Library of Congress Catalog Card Number: 65-19470.

[16] H. Burkhardt, M. Sippel, A. Herbertz, and J. Klevanski. "Comparative Study of Kerosene and Methane Propellant Engines for Reusable Liquid Booster Stages," Proceedings of the Fourth International Conference on Launcher Technology. Liège, Belgium, 3–6 December 2002.

[17] A. Abbud-Madrid, A. Modak, M. C. Branch, and J. W. Daily. "Combustion of Magnesium with Carbon Dioxide and Carbon Monoxide at Low Gravity." Journal of Propulsion and Power Vol. 17, No. 4, July–August 2001.

[18] Legrand, B., Marion, M., Chauveau, C., Gokalp, I., and Shafirovich, E., "Ignition and Combustion of Levitated Magnesium and Aluminum Particles and Carbon Dioxide," Combustion Science and Technology, Vol. 165, No. 1, 2001, pp. 151–174.

[19] M. K. King. "Simplified Two-Reaction Zone Model of Magnesium Combustion in Carbon Dioxide," Proceedings of the Combustion Institute, Vol. 29, No. 2, 2002, pp. 2931–2938.

[20] B. G. Drake, editor. "Human Exploration of Mars Design Reference Architecture 5.0," July, 2009. NASA-SP-2009-566.

[21] D. R. Williams. "Mars Fact Sheet". National Space Science Data Center. NASA. April 25, 2014.